Quantifying connectivity between mesophotic and shallow coral larvae in Okinawa Island, Japan: a quadruple nested high-resolution modeling study

Takeyasu, Kimika
Uchiyama, Yusuke
Mitarai, Satoshi

(Citation)
Frontiers in Marine Science,10:1174940

(Issue Date)
2023-04-24

(Resource Type)
journal article

(Version)
Version of Record

frontiers | Frontiers in Marine Science

TYPE Original Research
PUBLISHED 24 April 2023
DOI 10.3389/fmars.2023.1174940

OPEN ACCESS

EDITED BY
Andrea Cucco,
National Research Council (CNR), Italy

REVIEWED BY
Emmanuel Hanert,
Université Catholique de Louvain, Belgium
Yang Ding,
Ocean University of China, China

*CORRESPONDENCE
Yusuke Uchiyama
uchiyama@harbor.kobe-u.ac.jp

SPECIALTY SECTION
This article was submitted to Coastal Ocean Processes, a section of the journal Frontiers in Marine Science

RECEIVED 27 February 2023
ACCEPTED 05 April 2023
PUBLISHED 24 April 2023

CITATION
Takeyasu K, Uchiyama Y and Mitarai S (2023) Quantifying connectivity between mesophotic and shallow coral larvae in Okinawa Island, Japan: a quadruple nested high-resolution modeling study. *Front. Mar. Sci.* 10:1174940. doi: 10.3389/fmars.2023.1174940

Quantifying connectivity between mesophotic and shallow coral larvae in Okinawa Island, Japan: a quadruple nested high-resolution modeling study

Kimika Takeyasu[1], Yusuke Uchiyama[1]* and Satoshi Mitarai[2]

[1]Department of Civil Engineering, Kobe University, Kobe, Japan, [2]Marine Biophysics Unit, Okinawa Institute of Science and Technology Graduate University, Okinawa, Japan

Coral bleaching has recently been occurring extensively across the world's oceans, primarily because of high water temperatures. Mesophotic corals that inhabit depths of approximately 30–150 m are expected to survive bleaching events and reseed shallow water corals afterward. In Okinawa, Japan, mesophotic coral ecosystems have been reported to serve as a refuge for preserving the genotypic diversity of bleaching-sensitive corals. The connectivity of larval populations among different habitats is a key element that determines the area to be conserved in desirable coral ecosystems. Because coral larvae are largely transported passively by ambient oceanic currents, particularly in the horizontal direction, numerical ocean circulation models greatly help to quantify connectivity with detailed spatiotemporal network structures. The present study aimed to quantify the short-distance connectivity of shallow and mesophotic coral larvae in reef areas on the northwest coast of Okinawa Island. To this end, a quadruple nested high-resolution synoptic ocean model at a lateral spatial grid resolution of 50 m was developed, which was capable of realizing detailed coastal currents influenced by complex nearshore topography, and coupled with an offline 3-D Lagrangian particle-tracking model. After validating the developed model, short-distance horizontal coral connectivity across reef areas on the northwest coast was successfully evaluated. The alongshore lateral connectivity had apparent asymmetry caused by depth-dependent horizontal currents, whereas the larvae spawned at shallow and mesophotic depths were reachable to each other. Such across-depth larval dispersal was attributable to the mixed-layer depth in the spawning period, viz., the boreal spring, which approximately coincides with the boundary between shallow and mesophotic coral, leading to the intensive vertical exchange of virtual larvae.

KEYWORDS

mesophotic coral, connectivity, ocean circulation and particle tracking model, advective and dispersive effects, mixed layer

1 Introduction

Coral reefs are widely distributed along tropical and subtropical coasts and are composed of over 90,000 species that maintain a high biodiversity, resulting in coral reefs being recognized as one of the most important marine ecosystems on Earth. However, in recent years, overfishing, eutrophication, erosion, and climate change have led to the degradation of coral ecosystems globally (e.g., Hoegh-Guldberg et al., 2007; Carpenter et al., 2008; Hoegh-Guldberg et al., 2017; Hughes et al., 2018). High water temperatures occasionally lead to coral bleaching, which occurs extensively worldwide; for instance, in the Indian Ocean, Pacific Ocean, Red Sea, Caribbean Sea, and Great Barrier Reef (e.g., Lafratta et al., 2016; DeCarlo et al., 2017; Hughes et al., 2017).

Most coral research has focused on shallow corals, which are severely vulnerable to near-surface high temperatures, partly because they are more accessible and much less costly to observe than deep corals (e.g., Menza et al., 2008). Nevertheless, coral habitats have been confirmed to extend to deeper zones (Lesser et al., 2009; Hinderstein et al., 2010; Kahng et al., 2010), where the light intensity is only a fraction of that at the surface but is sufficient for zooxanthellae to live in symbiosis with corals for photosynthesis. Bongaerts et al. (2010) proposed the 'deep reef refugia hypothesis', which suggests that deep reef areas are protected or dampened from disturbances that affect shallow corals and may provide a viable reproductive source for shallow reef areas after disturbance. Recently, mesophotic coral ecosystems (MCEs; e.g., Kahng et al., 2014) that inhabit intermediate depths, ranging from approximately 30–150 m, called the mesophotic zone (MPZ), have drawn attention as potential refuges during high-temperature events under threats of coral bleaching. Mesophotic coral ecosystems consist of genetically similar species to shallow coral ecosystems and are expected to survive bleaching events due to the colder ambient temperature in the mesophotic depths and to reseed shallow corals afterward (e.g., Lesser et al., 2009; Bongaerts et al., 2010; Slattery et al., 2011). Similarly, MCEs are expected to be less susceptible to anthropogenic impacts and higher temperatures (Glynn, 1996; Hughes and Tanner, 2000; Lesser et al., 2009).

The Ryukyu Islands in the East China Sea (Figure 1) are located at a relatively high latitude compared with other coral habitats, hosting abundant coral reefs because of the influence of the warm Kuroshio Current (Ikeda et al., 2006). The archipelago was also affected by bleaching events in 2016. Kayanne et al. (2017) reported that ~90% of coral reefs at Ishigaki Island and 50–80% of coral reefs in Sekisei

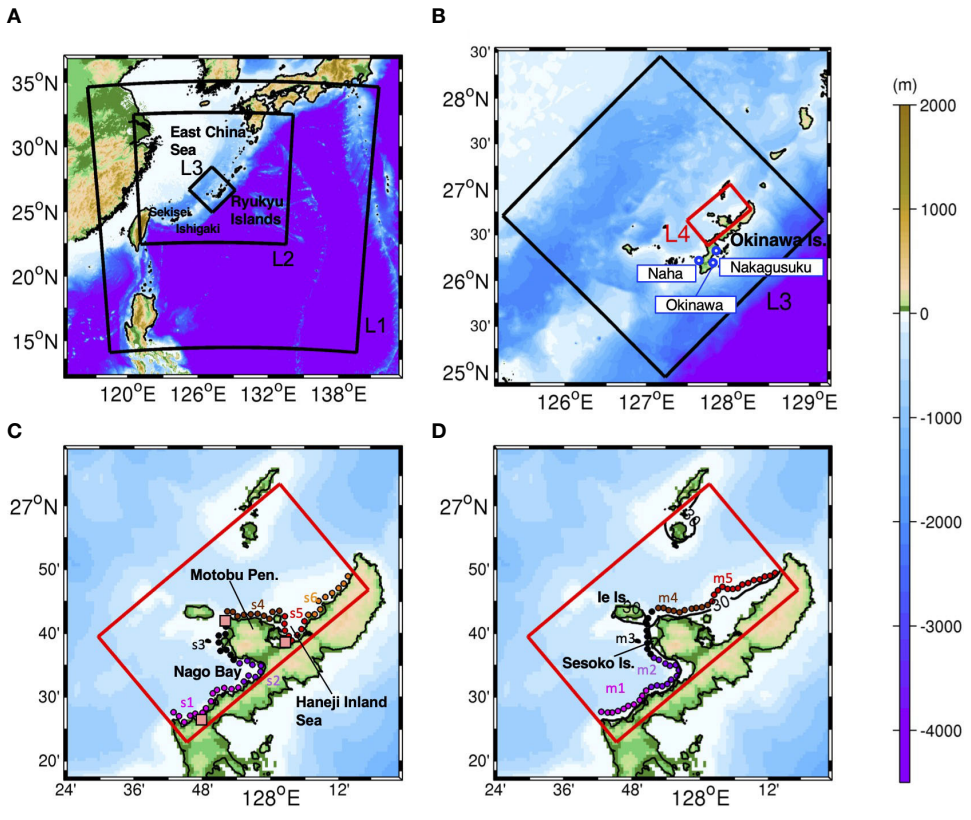

FIGURE 1
(A) The study area encompassing the entire Ryukyu Islands with the perimeter of the ROMS-L1, -L2, and -L3 models (black boxes), **(B)** and the ROMS-L4 model domain (red box) in the L3 domain (black box). Blue circles indicate the three tide gauge stations at Naha, Okinawa, and Nakagusuku discussed in section 2.4. **(C)** An enlarged plan view of the area around Okinawa Island with the source sites for particle tracking experiment Case 1 (shallow release from a depth of 2 m). The circles indicate 57 source and destination patches with a diameter of 500 m, which are further grouped into areas s1–s6. The pink squares indicate the virtual tide gauge stations for comparisons between the L3 and L4 tides in section 2.4. **(D)** Same as **(C)**, but for Case 2 (mesophotic release from a depth of ~30 m). The circles indicate 54 source and destination patches to be grouped into areas m1–m5. The black solid line is the isobath at a 30 m depth. The red rectangles correspond to the L4 domain in **(B–D)**. Colors show bathymetry in m.

Lagoon (Figure 1A) were damaged by this bleaching. The corals around Sesoko Island, located off the west coast of the Motobu Peninsula at Okinawa Island (Figures 1C, D), were critically affected by bleaching events in 1998 and 2001, resulting in the disappearance of bleaching-sensitive species, such as *Seriatopora hystrix*, from shallow water areas (van Woesik et al., 2011). However, Sinniger et al. (2013; 2017) found a brooding coral *S. hystrix* in the MPZ around Sesoko Island and speculated that MCEs could function as a buffer against thermal stress, thus, serve as a refuge to preserve the genotypic diversity of bleaching-sensitive corals. A vast area across the Ryukyu Islands is covered by bottom topographies suitable for the development of MCEs, such as deep terraces, banks, and pinnacles, potentially providing larger habitats than those for shallow corals. Indeed, multiple MCEs have been found in the Ryukyu Islands (Kimura et al., 2011; Fujita et al., 2012; Ohara et al., 2013; Sinniger et al., 2017), including those around Sesoko Island. Extensive surveys of deep corals could provide information regarding mesophotic corals around the Ryuku Islands, such as their distribution area, species, and connectivity (Sinniger and Harii, 2018).

A healthy and continuous supply of eggs and larvae is essential for coral persistence. It is necessary not only to maintain deteriorating coral habitats but also to preserve their spawning origins, as sufficient amounts of larvae must be recruited to sustain abundant coral ecosystems. Therefore, priority should be given to coral areas with ample and stable larval supplies. Population connectivity (or 'connectivity' for brevity) represents the statistical linkage of corals inhabiting different locations, evaluated based on the probability of their displacement due to Lagrangian advection by ambient oceanic currents (e.g., Mitarai et al., 2009). Thus, the connectivity of coral larval populations among different habitats is viewed as a key element determining the areas to be conserved (Munday et al., 2009). In particular, for mesophotic corals, vertical connectivity with shallow corals is an important factor that determines the health and fragility of MCEs. For instance, genetic analyses of *in situ* corals have verified vertical connectivity between shallow and mesophotic corals in Bermuda (Bongaerts et al., 2010), western and eastern Australia (Van Oppen et al., 2011), and the Red Sea (Kramer et al., 2019). Bongaerts et al. (2010) found that the reseeding potential of deep reefs varied among species and habitats and concluded that deep refugia should not be regarded as a broader ecosystem-wide phenomenon.

Coral larvae are generally passively transported to the surrounding currents in the ocean for days or even weeks after spawning because of their subtle swimming ability. Although the drifting larvae may be preyed on during this period, the survivors may sink to the ocean floor and attach themselves to hard surfaces, such as rocks and other hard corals, by chance. Hence, specification of the origin of the coral spawn as well as their habitat is essential to preserve coral ecosystems. Although numerical ocean models have been used to identify connectivity to complement genetic analyses, Thomas et al. (2015) first simulated larval dispersal and settlement at different depths, followed by Holstein et al. (2016) who used a biophysical model of larval dispersal to analyze the vertical connectivity of broadcasting and brooding species in the U.S. Virgin Islands and suggested the significance of mesophotic subsidies for shallow recruitment. However, there has been considerably less research on vertical connectivity than on horizontal connectivity (Holstein et al., 2016; Garavelli et al., 2018), and more importantly, studies on 3-D coral larval transport released from different depths are scarce and nil for Okinawa.

Connectivity has been evaluated based on population genetics, in which genetic similarities among individual corals sampled at different locations are diagnosed. On the other hand, a numerical ocean circulation model and Lagrangian particle-tracking model enable the quantification of connectivity with detailed spatiotemporal network structures. Uchiyama et al. (2018c) investigated the large-scale connectivity of coral larvae in reef areas across the Ryukyu Islands by focusing primarily on horizontal transport. Although the Kuroshio Current is expected to play a significant role in long-distance larval transport, where ~10% of the released larvae are transported extensively across the Ryukyu Islands, they showed that short-distance connectivity is quantitatively predominant for regional coral connectivity. However, they focused only on depth-integrated horizontal larval transport, thus, 3-D connectivity among multiple depths, including the MPZ, was not considered.

Based on the above arguments, this study aims to 1) investigate the 3-D, local, and short-distance transport of coral larvae released from different depths across coral reef areas on the northwest coast of Okinawa Island, including Seseko Island, where abundant mesophotic corals have been confirmed (Sinniger et al., 2017; Sinniger and Harii, 2018); 2) evaluate the vertical connectivity between shallow nearshore areas and mesophotic intermediate depth zones to demonstrate how significantly mesophotic corals are sustained by neighboring shallow corals, and vice versa; and 3) examine the mechanisms behind the formation of connectivity due to regional 3-D advective transport and vertical mixing effects. To this end, we conducted a quadruple nested high-resolution synoptic ocean modeling based on a highly sophisticated, state-of-the-art downscaling system (e.g., Kamidaira et al., 2017; Uchiyama et al., 2018c) coupled with a 3-D Lagrangian particle tracking model. An experiment was carried out for approximately 2 months, including the coral spawning period in the region, to quantify the short-distance and vertical transport of coral larvae in nearshore reef areas at a lateral spatial grid resolution of 50 m.

2 Methods

2.1 Downscaling 3-D ocean circulation model

Regional Oceanic Modeling System (ROMS; Shchepetkin and McWilliams, 2005; Shchepetkin and McWilliams, 2008) was used to develop a very high-resolution synoptic ocean model, *viz*., the ROMS-L4 model, at a lateral grid resolution of 50 m for the northwest coastal area of Okinawa Island (Figure 1). This resolution is required to represent detailed 3-D currents on the complex nearshore topography and bathymetry around the reef areas that are anticipated to influence short-distance and vertical larval transport. The outermost 3-D pelagic oceanic dynamics were provided by the assimilative Japan Coastal Ocean Experiment (JCOPE2) reanalysis product (Miyazawa et al., 2009). The one-way off-line nesting approach described in Mason et al. (2010) and

Uchiyama et al. (2018a) was applied to accomplish seamless multi-domain nesting with the combined Orlanski-type radiation condition and influx nudging condition towards the parent model output. This JCOPE2-ROMS downscaling system (Uchiyama et al., 2017b; Uchiyama et al., 2018a) has been used for several different Asian marginal seas with extensive validations against satellite and *in situ* observations (e.g., Kamidaira et al., 2018; Masunaga et al., 2018; Tada et al., 2018; Kamidaira et al., 2019; Kurosawa et al., 2020; Kamidaira et al., 2021; Zhang et al., 2022) and has been successfully extended to quadruple nested configurations with further downscaling (e.g., Uchiyama et al., 2018d; Zhang et al., 2019; Uchiyama et al., 2022).

The present ROMS-L4 model is embedded in the JCOPE2-ROMS model developed for the East China Sea, including the Ryukyu Islands, in double (Kamidaira et al., 2017; Uchiyama et al., 2018c; Takeda et al., 2021) and triple (Uchiyama et al., 2018b) nested configurations. The ROMS-L4 model was designed to encompass the northeast coast of Okinawa Island by 1386 × 800 horizontal grid cells and 32 vertically stretched terrain- and surface-following *s*-layers, covering an area of approximately 69.3 × 40 km. The model topography was obtained from the Shuttle Radar Topography Mission at 30-arc-sec resolution (SRTM30_Plus; Rodríguez et al., 2005; Becker et al., 2009), which covers the global ocean at 30 geographic arc-sec, supplemented by the Japan Oceanographic Data Center (JODC)-Expert Grid data for Geography at a 500 m resolution (http://www.jodc.go.jp/jodcweb/JDOSS/infoJEGG.html) for the coastal region. Surface wind stresses were imposed using the grid-point value mesoscale model (GPV-MSM), an operational atmospheric product of the Japan Meteorological Agency (JMA), at a horizontal resolution of 0.05° × 0.0625°. Net heat, freshwater, and radiation fluxes at the ocean surface were obtained from the Comprehensive Ocean-Atmosphere Data Set (COADS) of the National Oceanic and Atmospheric Administration (NOAA), a monthly climatology data with flux bias correction. Ten principal tidal constituents from the TPXO 7.0 global tidal reanalysis (Egbert et al., 1994; Egbert and Erofeeva, 2002) were additionally imposed on the sea-surface height along the perimeter of the ROMS-L2 model to include barotropic tides and resultant intrinsic baroclinic tides, which successively propagate into the child L3 and L4 models through the open boundaries. A short-term reanalysis was conducted for the 3-month period beginning on April 20, 2013 to properly include the timing of the synchronized mass spawning of coral in Okinawa, which typically occurs from late May to early June, excluding a model spin-up time of approximately 1 month prior to the main computation. Other computational conditions of the ROMS model suite for the Ryukyu Islands, including the present ROMS-L4 model, are summarized in Table 1.

2.2 Offline Lagrangian particle tracking model for ROMS

The 3-D Lagrangian transport of coral larvae was then numerically simulated using the precomputed 3-D flow field of the ROMS-L4 model output provided at 2 h intervals. An offline 3-D Lagrangian particle tracking model for ROMS was exploited (Carr et al., 2008), which has frequently been used in numerical studies on Lagrangian dispersal of virtual fluid parcels (e.g., Romero et al., 2013; Romero et al., 2016; Masunaga et al., 2022), larvae and eggs of marine fauna (Mitarai et al., 2009; Uchiyama et al., 2018b; Uchiyama et al., 2018c; Takeda et al., 2021), and even microplastic particles (Matsushita et al., 2022) with ample validations against *in situ* datasets of Lagrangian floats and drifters. Corals have various biological characteristics, such as larval behavior, larval pre-competency period, and larval reproduction duration, depending on their species, habitat, and other conditions (Shlesinger and Loya, 1985; Baird et al., 2009). However, little is currently known about corals in the study area, particularly mesophotic corals. Consequently, following on from previous researches of the study area (e.g., Uchiyama et al., 2018b; Uchiyama et al., 2018c), specific behavior models, such as diel vertical migration, mortality, or random walk subgrid-scale diffusivity, were not introduced to avoid further complexity and uncertainty. The present analysis purely pursued the advective effects of ambient flow fields on 3-D larval transport as simply as possible, as if coral larvae are passively

TABLE 1 Numerical configurations for the suite of the quadruple nested ROMS system.

Model	ROMS-L1	ROMS-L2	ROMS-L3	ROMS-L4
Computational period	1/1/2008 - 11/2/2015	12/27/2010 - 11/2/2015	10/11/2012 - 1/31/2014	4/20/2013 - 7/20/2013
Grids ($x \times y \times z$)	768 × 768 × 32 layers	1280 × 1120 ×32 layers	1088 × 1120 × 32 layers	1376 × 800 × 32 layers
Horizontal grid size	3.0 km	1.0 km	250 m	50 m
Baroclinic time step	240 s	40 s	15 s	1.5 s
Lateral B.Cs.	JCOPE2 (daily)	L1 (daily update)	L2 (2-hourly update)	L3 (2-hourly update)
Surface wind stress	GPV-GSM (6-hourly)	GPV-MSM (hourly)	GPV-MSM (hourly)	GPV-MSM (hourly)
Sea surface fluxes	COADS (monthly climatology)			
SST and SSS	JCOPE2 (10-day averaged)			
Tides	–	TPXO7	L2 (2-hourly update)	L3 (2-hourly update)
Topography	SRTM30_PLUS	SRTM30_PLUS (~1 km) + J-EGG500 (0.5 km)		

transported by oceanic currents. This approach is viewed as a basis for future research with detailed larval behaviors, such as vertical migration and subgrid-scale uncertainties.

The study area is topographically characterized by the Motobu Peninsula located in the middle of the model domain, which separates two sheltered shallow seas on both sides: Nago Bay on the left and Haneji Inland Sea on the right. For connectivity evaluation, coral habitats in the study area were defined as source and sink patches, as shown by the circle marks with a radius of 500 m in Figure 1. Approximately 500 virtual larvae were evenly distributed in each circular patch and were released from a depth of 2 m to represent shallow corals (Case 1) and from a depth of ~30 m to represent mesophotic corals (Case 2) by referring to the previous study (e.g., Holstein et al., 2016). Overall, 57 source patches were deployed in Case 1 (Figure 1C) and 54 in Case 2 (Figure 1D). Considering the regional topographic features, the 57 and 54 patches were grouped into six (Case 1) and five areas (Case 2) to identify the connectivity between the areas.

Releases of Lagrangian particles, viz., virtual coral spawning, occurred once a day at 00:00 for 1 month from May 20, 2013, which is the typical spawning time of corals in the study area. Hence, the total number of released Lagrangian particles was approximately 800,000 in each case. In general, the planula larvae of the corals survive for a few days to a few months before settlement. Nishikawa et al. (2003) reported that only 10% of the larvae of typical coral species in the study area can survive for 30 days after spawning. Therefore, particle tracking was conducted for up to 30 days after each release, until they were beached on a land grid, or until they exited the study area.

2.3 Lagrangian probability density functions and connectivity

To quantify the dispersal of Lagrangian particles released from source patches, Lagrangian probability density functions (PDFs) were analyzed following the methodology described by Mitarai et al. (2009). A Lagrangian PDF represents the PDF of particle displacement for a given elapsed time (i.e., advection time) τ as follows

$$f_X'(\boldsymbol{\xi};\tau,\boldsymbol{a}) = \frac{1}{N}\sum_{n=1}^{N}\delta(\boldsymbol{X}_n(\tau,\boldsymbol{a})-\boldsymbol{\xi}), \quad (1)$$

where N is the total number of particles, δ is the Dirac delta function, $\boldsymbol{X}_n$ is the position of the n-th Lagrangian particle, $\boldsymbol{a}$ is the initial position of the particle of interest, and $\boldsymbol{\xi}$ is the sample-space variable for $\boldsymbol{X}$. Both $\boldsymbol{a}$ and $\boldsymbol{\xi}$ encompass laterally over a circular patch with an arbitrary depth range in z. Discrete Lagrangian PDFs are evaluated from the center location of the release sites (patches) averaged over each site. Hence:

$$f_x'(\boldsymbol{\xi};\tau,\boldsymbol{a}) \approx \frac{1}{\pi R^2}\int_{|r|\le R} f_x'(\boldsymbol{\xi};\tau,\boldsymbol{a}+\boldsymbol{r})d\boldsymbol{r}, \quad (2)$$

where R is the radius of the release site $\boldsymbol{a}$. The final form of the discrete Lagrangian PDF is obtained by applying an isotropic spatial Gaussian filter, G:

$$f_x(\boldsymbol{\xi};\tau,\boldsymbol{a}) \approx \int_{-\infty}^{\infty} G(\boldsymbol{x}-\boldsymbol{\xi}) f_x'(\boldsymbol{\xi};\tau,\boldsymbol{a})d\boldsymbol{x}\,. \quad (3)$$

Coastal connectivity C_{ij} is defined as the probability of Lagrangian fluid particles being transported from source site i to sink site j over a time interval τ:

$$C_{ij}(\tau) = f_x(\boldsymbol{\xi}=\boldsymbol{x}_j;\tau,\boldsymbol{a}=\boldsymbol{x}_i)(\pi R^2), \quad (4)$$

where $\boldsymbol{x}_i$ and $\boldsymbol{x}_j$ are the source and sink patch locations, respectively, and normalization by πR^2 converts the PDFs into probabilities. The vertical coordinate z of $\boldsymbol{x}_i$ is 2 m (30 m) for shallow (mesophotic) releases from s1–s6 (m1–m5) for Case 1 (Case 2), as shown in Figure 1C (Figure 1D). The depth range of $\boldsymbol{x}_j$ was defined arbitrarily. For the depth-integrated Lagrangian PDFs and connectivity evaluated in section 3, $\boldsymbol{x}_j$ was defined with $-h < z \le \eta$, where h is the local depth and η is the free surface height. On the other hand, in section 4, $\boldsymbol{x}_j$ is defined with $-30 < z \le \eta$ (m) as the favorable depth zone to shallow corals and with $-150 < z \le -30$ (m) as that to mesophotic corals. Accordingly, the vertical connectivity between the shallow zones and MPZs was computed by adequately imposing the depth range constraints in $\boldsymbol{x}_i$ and $\boldsymbol{x}_j$. For further details on mathematical representations and their physical interpretations, refer to Mitarai et al. (2009).

2.4 Model validation

The parent models of the present multi-nested downscaling JCOPE2-ROMS system for the Ryukyu Islands have been thoroughly validated in previous studies to show the satisfactory reproducibility of the synoptic oceanic state and mesoscale variability (Kamidaira et al., 2017; Uchiyama et al., 2018c). The child ROMS-L4 model inherits a quantitatively similar reproducibility to that of its parent models. For instance, the modeled temperature was compared to observation to show high accuracy with the root mean square error of 0.906 °C and the model skill score of 0.935 (not shown). Here, the validation result of high-frequency tidal variability, which is a predominant driver of nearshore larval dispersal, is briefly presented. *In situ* tidal data at three tide gauge stations in Naha, Okinawa, and Nakagusuku were obtained from the JODC. Tidal harmonic analysis was then conducted for the data from January 1 to December 31, 2013. Figures 2A, B show scatterplots of the amplitudes and phase epochs of the four major principal tidal constituents (M_2, S_2, K_1, and O_1) computed from the observed data and the ROMS-L3 model output. The tidal amplitude and phases are well represented by the ROMS-L3 model, with correlation coefficients of 0.952 for the amplitude and 0.997 for the phase epoch. Subsequently, as no observed tidal data were available within the ROMS-L4 domain, another harmonic analysis was performed to compare the results of L3 and L4 models for 1 month of June, 2013 and showed extremely high correlations: 0.992 for amplitude and 1.000 for phase (Figures 2C, D). While the validation was conducted indirectly due to a shortage of *in situ* data, this result clearly shows that the ROMS-L4 model can reproduce tidal variability with high accuracy.

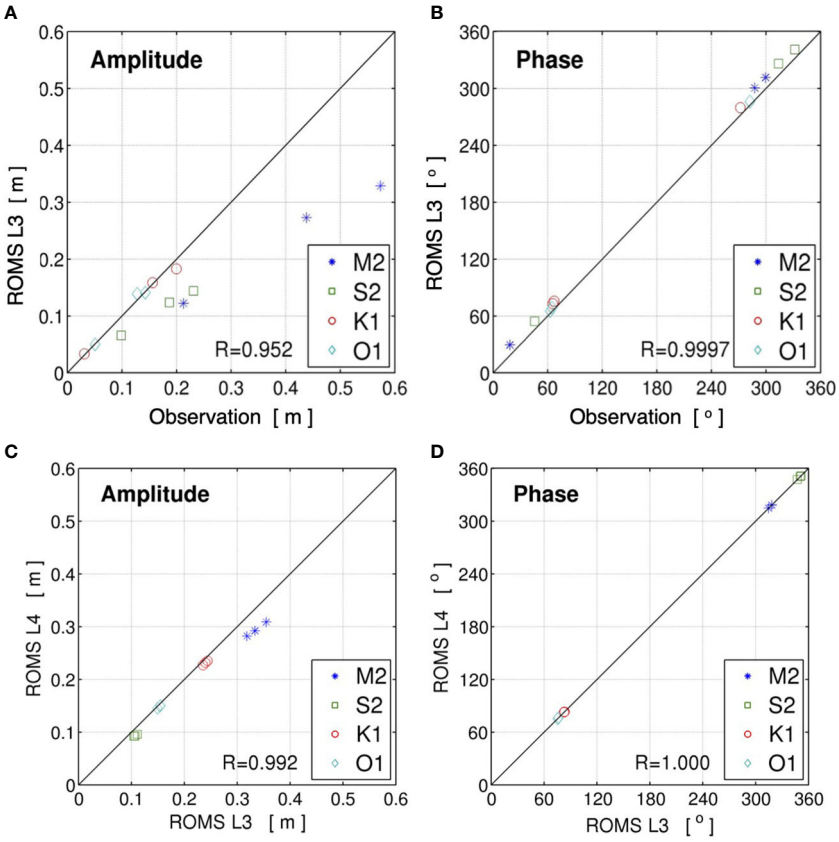

FIGURE 2
Scatter diagrams of the four major principal tidal constituents (M2, S2, K1, and O1) derived from harmonic analysis of the surface elevations. Upper panels show **(A)** the amplitude and **(B)** phase epoch from the ROMS-L3 and *in situ* observation at three tide gauge stations around the Okinawa Island shown by blue circles in Figure 1. Lower panels show **(C)** the amplitude and **(D)** phase epoch from the ROMS-L3 and ROMS-L4 models at the three virtual tide gauge stations shown by pink squares in Figure 1. R in each plot indicates the correlation coefficient.

3 Horizontal larval transport

3.1 Horizontal connectivity matrices

Figure 3 shows area-integrated connectivity matrices C_{ij} with the x-axis showing the source areas and the y-axis showing the destination areas on the labeled advection time (T_a) in days. The upper panels show the Lagrangian particles representing shallow coral larvae released from a depth of 2 m (Case 1), while the lower panels show the particles representing mesophotic coral larvae released from a depth of 30 m (Case 2). For brevity, hereinafter, the former particles are referred to as '(virtual) shallow coral larvae', while the latter is referred to as '(virtual) mesophotic coral larvae'. For example, the combination of the x-axis of s4 and y-axis of s3 at T_a = 5 days in Figure 3A shows yellowish green, viz., $C_{s4s3} \cong 10^{-3}$, which can be interpreted as one coral larva out of 1,000 released from the s4 area (northeastern shore of the Motobu Peninsula; Figure 1) can be transported to the s3 area (the western shore of Motobu Peninsula) in 5 days.

Both Case 1 and 2 initially exhibit higher connectivity around the line with the 45° slope depicted by reddish colors until the advection time of 14 days, showing that lateral dispersal is not that extensive, and the released virtual larvae largely stay near the source areas for the first 2 weeks. Particularly in highly sheltered areas, such as s2, m2 (Nago Bay), and s5 (Haneji Inland Sea), most larvae remain near the source areas and self-recruitment is predominant. Although they are dispersed gradually as the advection time progresses, the larvae originating from the source areas s2, m2 and s5 are retained near the source area with a connectivity of over 10^{-3} even at T_a = 30 days.

A significant difference between the two cases is found in the along-isobath connectivity between the northeastern and southwestern areas of the Motobu Peninsula. The connectivity near the lower right corners of the matrices (e.g., C_{ij} with i = s4, s5, and s6, and j = s1, s2, and s3) is generally small for shallow coral larvae (Case 1) at all three T_a, demonstrating that southwestward larval transport beyond the Motobu Peninsula is rare. However, for mesophotic coral larvae released from a depth of 30 m (Case 2), the connectivity around the lower right corner of the matrices is higher than that in Case 1, indicating that more larvae are transported southwestward (i.e., from Haneji Inland Sea to Nago Bay) in the MPZ. Therefore, this result suggests that horizontal larval connectivity differs depending on the released depths, particularly on the northern (Haneji) side of the Motobu Peninsula.

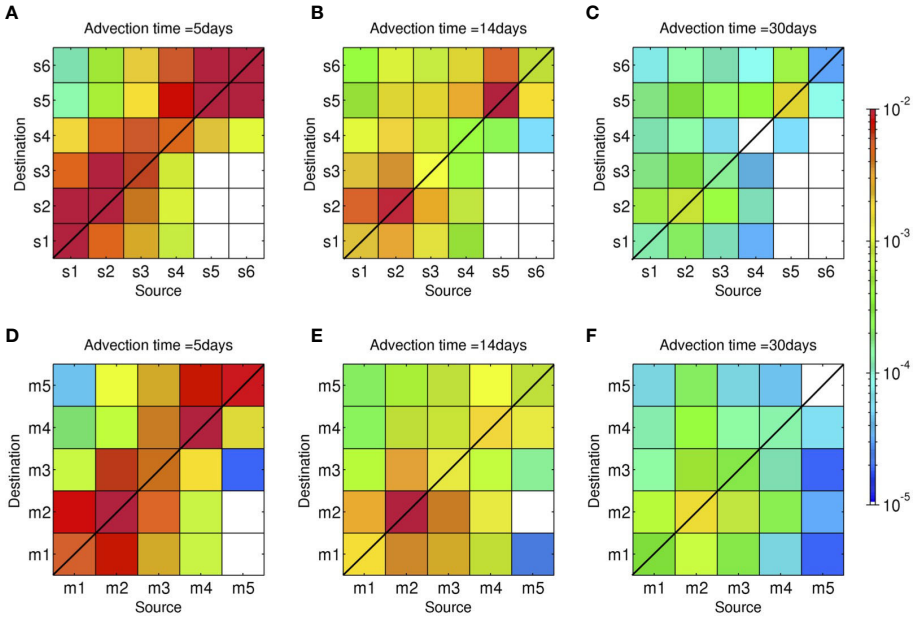

FIGURE 3
Horizontal connectivity matrices around the northwest coast of Okinawa Island for the advection times T_a of 5, 14, and 30 days. Colors indicate the probability, viz., connectivity C_{ij}. The x-axes show the grouped source areas, and the y-axes show the grouped sink areas shown in Figure 2. Upper panels **(A–C)**: shallow connectivity matrices for releases at a depth of 2 m (Case 1). Lower panels **(D–F)**: mesophotic connectivity matrices for releases from a depth of 30 m (Case 2).

3.2 Depth-integrated Lagrangian PDFs

Figure 4 shows the temporal evolution of the depth-integrated (viz., ξ is defined over the entire depth range $-h < z \leq \eta$. See section 2.3) Lagrangian PDF distribution of virtual larvae released from areas s2 and s6 (at a 2 m depth) and area m5 (at a 30 m depth) at advection times of 5, 14, and 30 days, illustrating depth-independent lateral transport patterns of shallow coral larvae (six panels in the upper two rows) and mesophotic coral larvae (bottom panels). The higher the Lagrangian PDF, the more particles are transported to that location. The vast majority of shallow coral larvae released from the semi-enclosed Nago Bay (area s2) remains around the source area at T_a = 5 days (Figure 4, top panels), suggesting that short-term self-recruitment plays an important role in the formation of recognizable local connectivity in such sheltered areas. Consistent with the temporal evolution of the connectivity shown in Figures 3A–C, the larvae from s2 are transported and dispersed to surrounding areas gradually over the advection time in both the northeastward and southwestward directions with substantial retention to the source areas.

The middle and bottom panels of Figure 4 compare the Lagrangian PDFs of the virtual larvae released from source areas s6 (shallow corals) and m5 (mesophotic corals) located off the northeastern coast of the Motobu Peninsula. Prevailing northeastward transport and a subsequent exit from the L4 domain are evident regardless of the release depth, although there is modest reversal of larval transport beyond the peninsula. This reversed southwestward transport to the other side of the peninsula is more apparent for the larvae from m5 (mesophotic corals) than for those from s6 (shallow corals) because of the along-isobath transport in the deeper offshore areas, whereas the larvae from s6 are entrained in the shallower area in the Haneji Inland Sea around area s5.

Figure 5 shows fractions of the virtual larvae transported from the northeastern side of the Motobu Peninsula (areas s4–s6 and m4–m5) to the other side (area A in Figure 6) as a function of the advection time. The fractions of the reverse transport based on all the released larvae (blue curves) from the shallow zones and the MPZs increase in the first few days, and then gradually decrease. However, the difference is found to be insignificant by ~1%, or by ~3,750 Lagrangian particles, because the majority of the larvae that originate from the northeastern areas are transported northeastward out of the study area through the eastern open boundary. In contrast, the fractions based on the particles remaining in the study area (red curves, F_{remain}) are found to be significantly different between the shallow and mesophotic release cases. At the advection time of 30 days, only ~12% of the larvae released from the shallow areas (red dotted curve) reaches area A (see Figure 6) on the other side of the peninsula, whereas more southwestward reverse transport beyond the peninsula is found for the larvae released from the mesophotic areas of ~33% (red solid curve). These results well-quantify the visual patterns of the Lagrangian PDFs shown in Figure 5.

3.3 Horizontal current field

In the preceding two subsections, the release depth was demonstrated to alter horizontal larval transport. To examine the mechanism behind the difference in the horizontal transport

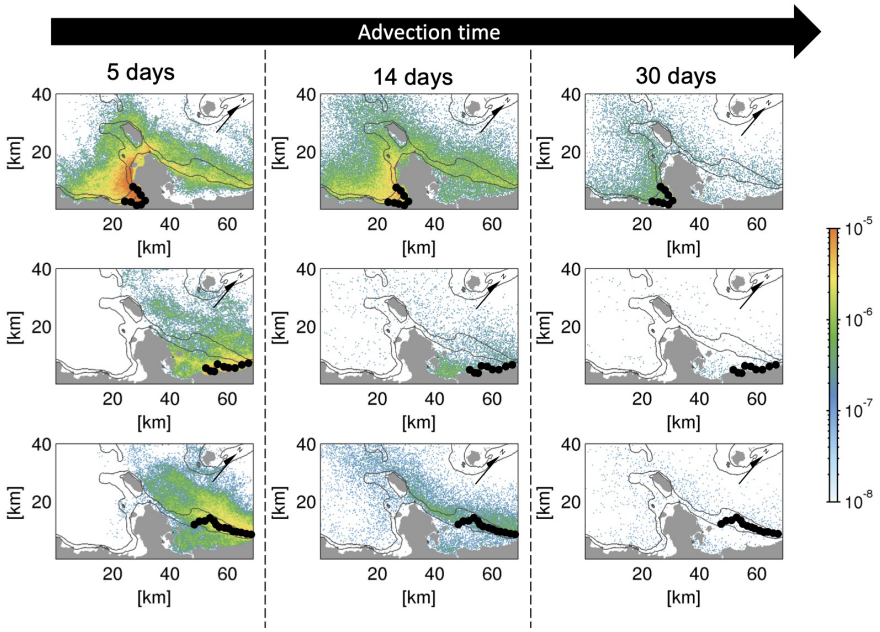

FIGURE 4
Temporal evolution of depth-integrated horizontal Lagrangian PDFs (color) released from (top) areas s2, (middle) s6, and (bottom) m5 at the labeled advection time T_a (days). Black circles indicate the source patches of each release area. The black solid contours are the isobaths of 30 and 100 m depths. Arrows point to the true north as the panels are rotated relative to the geographical coordinates.

patterns of the larvae released from the two depth zones, the monthly averaged flow fields near the surface at a 5 m depth and around the mesophotic layer at a 40 m depth are depicted in Figures 6A, B. The near-surface currents (Figure 6A) indicate that a pronounced northeastward velocity exceeding 0.2 m/s develops on the northeastern side of the Motobu Peninsula, consistent with the dominant transport direction of the shallow coral larvae released from area s6 (Figure 4, middle panels). It should be noted that larval transport opposite to the mean current direction is induced by residual and dispersive effects associated with tidal currents and other high-frequency factors. On the southwestern side of the peninsula (Nago Bay), the surface currents are characterized by nearshore anticyclonic, clockwise circulation that extends to the northward flow around the peninsular tip and is part of the northeastward flow on the other side (Haneji Inlans Sea). Stagnated water is formed in Nago Bay, where shoreward retention is promoted for the shallow larvae released from area s2 with overall northeastward transport to the other side of the peninsula (Figure 4, top panels).

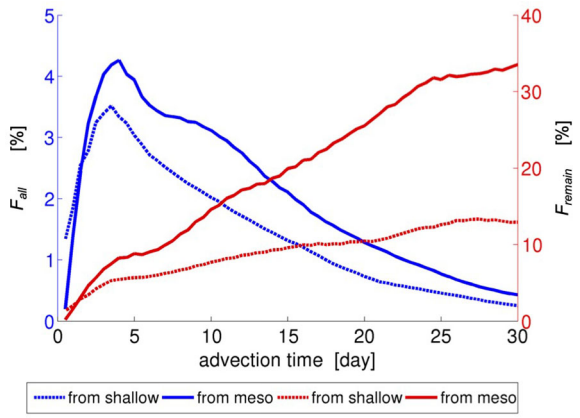

FIGURE 5
Fractions (%) of the virtual larvae transported from the northeastern side of the Motobu Peninsula (areas s4–s6 and m4–m5) to the other side (area A in Figure 6C) as a function of the advection time. F_{all} (blue curves): fractions of all the released larvae. F_{remain} (red curves): fractions of the larvae that remain in the study area (viz., those that have not exited). The dotted curves pertain to Case 1 (shallow release) and the solid curves pertain to Case 2 (mesophotic release).

Meanwhile, the mesophotic current distribution at a depth of 40 m (Figure 6B) resembles the near-surface current distribution, although it is much weaker. The most striking difference is the bathymetric constraint at the peninsular tip, which blocks the mesophotic currents from passing through. In turn, westward currents are formed from the peninsular tip towards Ie Island (the island just off the peninsular tip), resulting in westward elongated PDFs of the mesophotic larvae from m5 until T_a = 14 days, followed by modestly higher PDFs in area A at T_a = 30 days (Figure 4, bottom panels) than those of the shallow larvae from s6. In addition, the mesophotic larvae from m5 are transported shoreward to reach shallow areas of the Hanaji Inland Sea, where the depth is shallower than 40 m, as depicted by the nil velocity colored in white in Figure 6B. In addition to the bathymetric constraint, the surface mixed layer plays an inevitable role in dynamically decoupling shallow and mesophotic currents. The surface mixed-layer depth H_{bls} evaluated using the KPP turbulence model in ROMS (Figure 6C) ranges 15–25 m in offshore areas, which separated the near-surface currents and

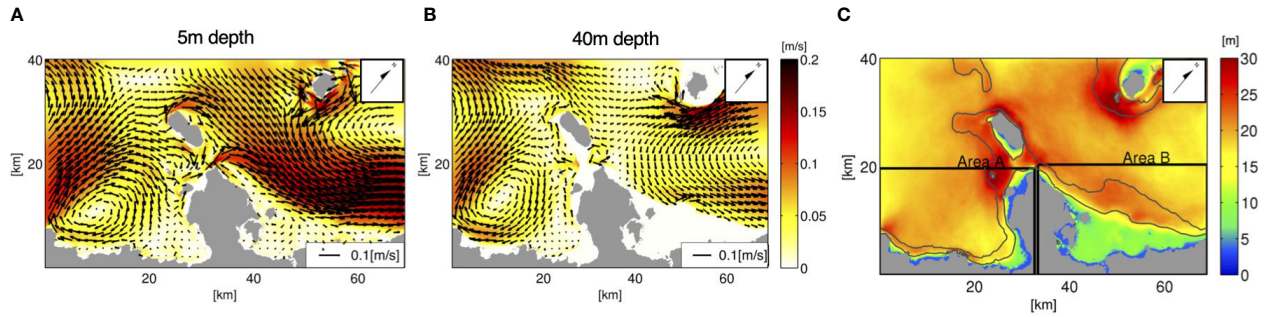

FIGURE 6
Time-averaged flow fields based on the ROMS-L4 model output for the 1-month period of June, 2013. The horizontal velocity vectors **(A)** at a 5 m depth (near-surface) and **(B)** at a 40 m depth (mesophotic zone), overlaid on their absolute values (m/s) indicated by color, are depicted. **(C)** The surface mixed-layer depth H_{bls} (m) is indicated by color, with the two black rectangles showing areas A and B used for the analyses in sections 3.2 and 4.2. The black solid contours indicate the isobaths of 30 and 100 m depths. Arrows point to the true north.

associated shallow coral larval transport from those in the mesophotic layer. In contrast, when H_{bls}< 10 m or $H_{bls} \approx h$ in shallow nearshore areas, vertical eddy mixing considerably promotes vertical larval exchange.

4 Three-dimensional larval transport

4.1 Three-dimensional connectivity between shallow zones and MPZs

In this study, the horizontal transport of virtual larvae released from shallow source sites (s1–s6) and mesophotic source sites (m1–m5) were examined using depth-independent Lagrangian PDFs and associated connectivity. To further understand the connection between the two depth zones, the 3-D connectivity is evaluated at advection times of 5, 14, and 30 days, as summarized in Table 2. Here, the source/destination areas are s1–s6 for the shallow larvae and m1–m5 for the mesophotic larvae, whereas the destination areas are further restricted to the two depth zones. As explained in section 2.3, the depth range of the destination patch x_j was taken as -30 (m) $< z \leq \eta$ for the shallow coral settlement at s1–s6, and as $-150< z \leq -30$ (m) for the mesophotic coral settlement at m1–m5 (Figure 7). The 3-D connectivity is the area-integrated value for a given depth range in x_j. For instance, (3) shallow-mesophotic connectivity is computed from the larvae released from the source areas s1–s6 (with a release depth of 2 m) that reach the destination areas m1–m5, but only within the mesophotic depth range of $-150< z \leq -30$ (m).

Table 2 clearly illustrates that vertical connectivity (3) and (4) is significant, whereas horizontal connectivity (1) and (2) is 2–3 times as large. All the 3-D connectivity values decrease with time, but at T_a = 14 days, they are still 1/3–2/3 of those at T_a = 5 days. Then, these values further decrease to almost zero at T_a = 30 days, as the larvae are mostly flushed out of the study area, while the vertical connectivity values (3) remain as large as those of horizontal connectivity. More interestingly, the vertical connectivity from the mesophotic to the shallow zone (4) is higher than that from the shallow to MPZ (3) until T_a = 14 days, and is quantitatively comparable to the horizontal connectivity within the MPZ (2). Therefore, the MPZ is deemed to be an important source for both mesophotic and shallow coral ecosystems. Similarly, the shallow zone could also be a source for both depth zones but to a lesser degree.

4.2 Vertical distribution of Lagrangian PDFs

To investigate a possible mechanism that promotes vertical connectivity between the shallow zones and MPZs, temporal evolutions of the vertical distribution of Lagrangian PDFs of the virtual larvae integrated over areas A and B (see Figure 6C) are depicted with the surface mixed-layer depth H_{bls} (solid line: spatiotemporal average and dotted lines: standard deviations $\pm\sigma$)

TABLE 2 Three-dimensional connectivity between two depth zones at the advection times T_a of 5, 14, and 30 days.

	Advection time, T_a		
Source-destination types	5 days	14 days	30 days
(1) Shallow-shallow	3.96×10^{-2}	1.23×10^{-2}	1.24×10^{-3}
(2) Mesophotic-mesophotic	2.18×10^{-2}	7.78×10^{-3}	1.29×10^{-3}
(3) Shallow-mesophotic	6.13×10^{-3}	4.41×10^{-3}	9.83×10^{-4}
(4) Mesophotic-shallow	1.84×10^{-2}	6.21×10^{-3}	4.39×10^{-6}

(1) Source: shallow zone and destination: mesophotic zone, (2) source: mesophotic and destination: mesophotic, (3) source: shallow and destination: mesophotic, and (4) source: mesophotic and destination: shallow. (1) and (2) represent horizontal connectivity, while (3) and (4) represent vertical connectivity.

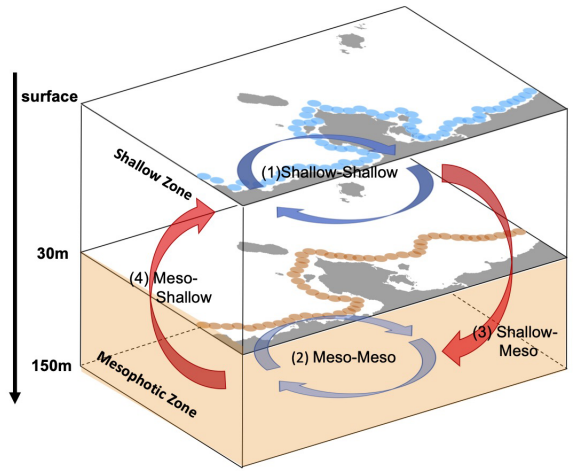

FIGURE 7
Schematic diagram of four types of the horizontal and vertical connectivity between the shallow corals and the mesophotic corals. Blue and orange circles are the source patches used for Case 1 (Figure 1C) and Case 2 (Figure 1D), respectively. In this study, the shallow zone is defined from the surface down to 30 m depth, while the mesophotic zone is from 30 m to 150 m depths. Mesophotic is abbreviated to "Meso" here. See also Table 2.

in Figure 8. Strikingly, the mixed layer constrains the vertical extent of the virtual larvae. For the larvae released from a 2 m depth (Case 1, Figures 8A, C), most of the larvae stay above the base of the mixed layer at approximately $-18 < z \leq -23$ (m), which reduces the number of near-surface larvae that sink. As a result, in both areas, the Lagrangian PDFs near the surface are ~10^{-2}, while they are lowered to ~10^{-3} at ~40 m, which is one order of magnitude smaller. Near-surface retention is more apparent with less downward dispersion in area B than in area A because of extensive shallow nearshore areas in area B that lead to a shallower H_{bls} (Figure 6C), which impedes downward larval transport.

However, for the mesophotic coral larvae released from a depth of 30 m (Case 2, Figures 8B, D), the Lagrangian PDF peaks at roughly the same release depth. They are vertically dispersed to be extended down to an ~80 m depth with PDFs of ~5.0×10^{-4}, meaning that only one larva out of 2,000 reaches this depth. Initial dilution takes place in approximately 1 day when a small fraction of mesophotic larvae is entrained in the mixed layer and moves upward to the surface. Because of the restricted downward transport of near-surface larvae across H_{bls}, the surfaced mesophotic larvae dominate over the subsurface larvae as the advection time progresses. This is more evident in area B (Figure 8D), where shallow sheltered areas in the Hanaji Inland Sea intensify near-surface retention (Figure 4).

Mesophotic coral spawning was set to occur at a depth of 30 m from May to June to suit the timing of mass spawning in the study area, corresponding to the boreal spring when the surface mixed-layer develops to approximately 15–25 m from the surface. Thus, the release depth of mesophotic coral larvae coincides with the vertical range of the seasonally varying surface mixed-layer depth in the area. Therefore, the mixed layer plays two important roles in: 1) acting as a barrier that prevents shallow (mesophotic) coral larvae from being transported downward (upward), and 2) enhancing near-surface vertical mixing to accumulate larvae near the surface. If spawning occurs in the middle of summer, when H_{bls} is much shallower, role 1) as a barrier prevails to diminish vertical larval exchange between the shallow zones and MPZs.

5 Discussion

In the present study, the competency period was simply considered for determining the analysis period, but other details

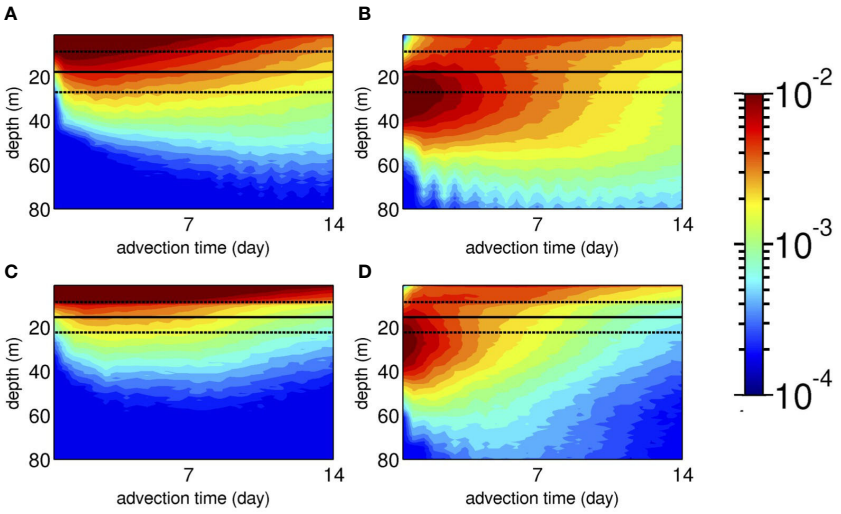

FIGURE 8
Hovmöller plots of the vertical distribution of the Lagrangian PDFs integrated over **(A, B)** area A and **(C, D)** area B (see Figure 6C for the definition) as a function of the advection time until T_a = 14 days (colors). Left panels **(A, C)**: Case 1 with shallow releases from a depth of 2 m. Right panels **(B, D)**: Case 2 with mesophotic releases from a depth of 30 m. The solid black lines indicate the mean surface mixed-layer depth H_{bls} averaged temporally for 1 month of June 2013 and spatially over each area A and B (see Figure 6C), and the dotted black lines indicate the ranges of their standard deviations, $\pm \sigma$.

of coral life history, such as vertical migration, mortality, and density, were not considered because of the high degree of uncertainty involved. However, the density of coral larvae usually changes during their swimming period (Arai et al., 1993; Szmant and Meadows, 2006; Vermeij et al., 2006), and a certain number of larvae die while floating in the ocean without reaching the bottom (Graham et al., 2009). Biophysical particle tracking computational modeling studies have shown that incorporating a biological model does not change relative connectivity patterns, but that diel vertical migration and mortality significantly affect absolute connectivity (Garavelli et al., 2018). In addition, we presumed mesophotic corals are spawned at a depth of 30 m based on the preceding study by Holstein et al. (2016), and vertical random-walk diffusivity is not considered for sake of simplicity, whereas these two factors may affect vertical distribution to some extent. Although there remain many unanswered questions regarding the effects on the vertical distribution of coral larvae compared to those on the horizontal distribution, it is possible that adopting the spontaneous vertical migration pattern of larvae in the model could increase the number of particles reaching the surface after spawning at depth and further enhance connectivity between the shallow zones and MPZs. Therefore, studies on the biology and life history of corals inhabiting the study area are expected to enable more detailed and realistic modeling studies, which could be accomplished by improving the present particle tracking model to an individual-based biological model (e.g., Fujimura et al., 2014; Thomas et al., 2015).

As a relatively high-resolution model was employed with a horizontal grid resolution of 50 m here, our focus is on the three-dimensional transport process among offshore areas rather than on detailed behavior within the reef. Nevertheless, it is believed that understanding inner reef circulation is also important for estimating local coral recruitment. Indeed, it has been confirmed that nearshore circulation in many coral reefs, such as in the Indian Ocean, Pacific Ocean, and Caribbean Sea (Munk and Sargent, 1948; Symonds et al., 1995; Hearn, 1999; Hench et al., 2008; Lowe et al., 2009), is mainly affected by breaking waves. Other wave effects, such as Stokes drift, wave setup, wave-driven nearshore currents, breaker-enhanced turbulent mixing, and wave-induced bottom streaming (e.g., Uchiyama et al., 2009; Uchiyama et al., 2010; Weir et al., 2011; Marchesiello et al., 2015; Uchiyama et al., 2017a; Akan et al., 2020; Wang et al., 2020; Wang et al., 2021), are also anticipated to significantly influence Lagrangian transport in coastal areas. The linear addition of Stokes drift to the Lagrangian equation of motion of the particle tracking models has been reported to improve reproducibility in the open ocean to a certain extent (e.g., Iwasaki et al., 2017; Matsushita et al., 2022). Nearshore currents, in particular transient rip currents (e.g., Fujimura et al., 2017; Uchiyama et al., 2017a; Fujimura et al., 2018), which occur intermittently and promote cross-shore exchange and dispersal extensively, must be considered to represent inter-reef larval transport. However, the inclusion of wave effects is beyond the scope of the present study, partly because the present grid resolution of 50 m is insufficient to properly represent the surf zone, and further nesting should be conducted to develop a much higher-resolution model that accounts for the surf zone dynamics accurately. This will be pursued in the future with our ROMS model, which has already been equipped with sophisticated functionality to include wave effects to simulate nearshore circulation (Uchiyama et al., 2010), thus, enabling more realistic larval transport modeling across the inner and outer areas of multiple coral reefs.

6 Conclusions

The 3-D inter-reef connectivity of coral larvae was numerically investigated for the northwestern coastal area of Okinawa Island, located in the East China Sea, using an offline Lagrangian particle tracking model driven by a quadruple nested high-resolution JCOPE2-ROMS downscaling model (e.g., Uchiyama et al., 2018c). Coral larvae were modeled to inhabit the shallow zone at a depth of 2 m and the MPZ at a depth of 30 m. It was found that short-distance, local connectivity within the source areas was as high as $\sim 10^{-2}$ in the first few days, which was 10 to 100 times higher than the connectivity in other areas. This pronounced initial self-recruitment gradually decreased as the advection time T_a progressed, and the virtual larvae were transported to other areas away from the source areas. For example, the self-recruitment connectivity within the southwestern-most shallow area s1 (Figure 1C), C_{s1s1}, was evaluated to be $\sim 10^{-2}$ at T_a = 5 days, while it decreased to $\sim 10^{-4}$ at T_a = 30 days (Figure 3). Meanwhile, the high-resolution model allowing the representation of detailed topographic features indicated the sizable entrainment of larvae in sheltered areas, such as Nago Bay (areas s2 and m2 in Figures 1C, D) and Haneji Inland Sea (area s5 in Figure 1C), where connectivity remained as high as 10^{-3} even at T_a = 30 days.

For the horizontal transport of the shallow coral larvae, northeastward inter-reef transport beyond the Motobu Peninsula (e.g., from s1–s2 to s5–s6) was predominant with a connectivity of $\sim 1–4 \times 10^{-4}$ (Figure 3C) at T_a = 30 days, whereas the opposite transport (e.g., from s5–s6 to s1–s2) barely occurred with connectivity of less than 10^{-5} or a fraction of ~12% (Figure 5). This significant directional bias was well-explained by vigorous mean northeastward near-surface currents at 0.1–0.2 m/s developed more energetically on the northeastern side of the peninsula (Figure 4A). In contrast, for the mesophotic coral larvae, the opposite transport (e.g., from m4–m5 to m1–m2) occurred more evidently by $\sim 3 \times 10^{-4}$ (Figure 3D) or ~33% (Figure 5) at T_a = 30 days than the shallow coral larvae. Even with the subsurface topographic barrier near the peninsular tip in the MPZ, less energetic northeastward currents on the northeastern side and moderate westward currents near the tip (Figure 4B) jointly promoted the southwestward transport of the larvae released from the MPZ. Therefore, lateral connectivity was established asymmetrically in the alongshore direction around the peninsula, although the bias was largely influenced by the seasonal surface mixed-layer (Figure 4C) and associated depth-dependent horizontal currents.

It was also found that the virtual larvae released in the shallow zones and MPZs were interchangeable (Table 2). The vertical range of the mixed-layer depth H_{bls} for the boreal spring in the study area

and the presumed broadcast spawning depth of the mesophotic coral overlapped at a ~30 m depth. This coincided with the enhanced upward entrainment of mesophotic coral larvae to emerge near the surface where shallow corals coexist (viz., predominance of 3-D connectivity (4) from the MPZ to the shallow zone in Table 2) under the influence of intensive vertical mixing in the surface mixed layer (Figure 8). The larvae released from the MPZ also dispersed vertically down to the deeper zone below the mixed layer, while upward transport occurred to induce both shallow and mesophotic corals to remain in the surface zone. Conversely, the mixed layer extending to the MPZ promoted the shallow corals to sink down, leading to modest vertical connectivity from the shallow zone to the MPZ (viz., 3-D connectivity (3) in Table 2) to a much lesser degree than (4). In conclusion, the above results suggest the significance of 3-D connectivity between mesophotic and shallow coral ecosystems. Hence, yet with several technical limitations argued in Section 5, the present study confirmed that the mesophotic coral ecosystem could serve as a refuge from environmental stresses for shallow corals in the study area under advective effects of the ambient 3-D currents.

Data availability statement

The ROMS model used in this study is distributed by its developers and is available at https://www.myroms.org/. The JCOPE2 reanalysis data are available for scientific research purposes from Japan Agency for Marine-Earth Science and Technology (JAMSTEC) and are available at http://www.jamstec.go.jp/jcope/htdocs/e/distribution/index.html. The STRM30_Plus data are available at https://topex.ucsd.edu/WWW_html/srtm30_plus.html. The J-EGG500 data set is distributed by JODC at https://www.jodc.go.jp/jodcweb/JDOSS/infoJEGG.html. The GPV-GSM and GPV-MSM atmospheric products were generated by JMA and are available from the repository at http://database.rish.kyoto-u.ac.jp/arch/jmadata/data/gpv/original/. The COADS data are maintained and distributed by NOAA at https://psl.noaa.gov/data/gridded/data.coads.1deg.html. The present ROMS-L4 model was built upon parent models developed with earnest assistance from Yuki Kamidaira, Sachika Odani, and Tsubasa Miyagawa. Further inquiries can be directed to the corresponding author.

Author contributions

KT: Investigation, Software, Validation, Visualization, Writing – original draft. YU: Conceptualization, Methodology, Supervision, Software, Writing- Reviewing and Editing, Funding acquisition. SM: Methodology, Investigation. All authors contributed to the article and approved the submitted version.

Funding

This research was financially supported by the Japan Society for the Promotion of Science (JSPS) Grant-in-Aid for Scientific Research (Grant # 18H03798) at Kobe University.

Conflict of interest

The authors declare that the research was conducted in the absence of any commercial or financial relationships that could be construed as a potential conflict of interest.

Publisher's note

References

Akan, C., McWilliams, J. C., and Uchiyama, Y. (2020). Topographic and coastline influences on surf eddies. *Ocean Modell.* 147, 101565. doi: 10.1016/j.ocemod.2019.101565

Arai, I., Kato, M., Heyward, A., Ikeda, Y., Iizuka, T., and Maruyama, T. (1993). Lipid composition of positively buoyant eggs of reef building corals. *Coral Reefs* 12, 71–75. doi: 10.1007/BF00302104

Baird, A. H., Guest, J. R., and Willis, B. L. (2009). Systematic and biogeographical patterns in the reproductive biology of scleractinian corals. *Annu. Rev. Evol. Syst.* 40, 551–571. doi: 10.1146/annurev.ecolsys.110308.120220

Becker, J. J., Sandwell, D. T., Smith, W. H. F., Braud, J., Binder, B., Depner, J., et al. (2009). Global bathymetry and elevation data at 30 arc seconds resolution: SRTM30_PLUS. *Mar. Geodesy* 32 (4), 355–371. doi: 10.1080/01490410903297766

Bongaerts, P., Ridgway, T., Sampayo, E. M., and Hoegh-Guldberg, O. (2010). Assessing the 'deep reef refugia' hypothesis: focus on Caribbean reefs. *Coral Reefs* 29, 309–327. doi: 10.1007/s00338-009-0581-x

Carpenter, K. E., Abrar, M., Aeby, G., Aronson, R. B., Banks, S., Bruckner, A., et al. (2008). One-third of reef-building corals face elevated extinction risk from climate change and local impacts. *Science* 321, 560–563. doi: 10.1126/science.1159196

Carr, S. D., Capet, X. J., McWilliams, J. C., Pennington, J. T., and Chavez, F. P. (2008). The influence of diel vertical migration on zooplankton transport and recruitment in an upwelling region: estimates from a coupled behavioral-physical model. *Fish. Oceanogr.* 17, 1–15. doi: 10.1111/j.1365-2419.2007.00447.x

DeCarlo, T. M., Cohen, A. L., Wong, G. T., Davis, K. A., Lohmann, P., and Soong, K. (2017). Mass coral mortality under local amplification of 2 c ocean warming. *Sci. Rep.* 7, 44586. doi: 10.1038/srep44586

Egbert, G. D., Bennett, A. F., and Foreman, M. G. (1994). TOPEX/POSEIDON tides estimated using a global inverse model. *J. Geophys. Res.* 99, 821–824, 852. doi: 10.1029/94JC01894

Egbert, G. D., and Erofeeva, S. Y. (2002). Efficient inverse modeling of barotropic ocean tides. *J. Atmos. Ocean. Tech.* 19 (2), 183–204. doi: 10.1175/1520-0426(2002)019<0183:EIMOBO>2.0.CO;2

Fujimura, A. G., Reniers, A. J. H. M., Paris, C. B., Shanks, A. L., MacMahan, J. H., and Morgan, S. G. (2014). Numerical simulations of larval transport into the surf zone. *Limnol. Oceanogr.* 59, 1434–1447. doi: 10.4319/lo.2014.59.4.1434

Fujimura, A. G., Reniers, A. J. H. M., Paris, C. B., Shanks, A. L., MacMahan, J. H., and Morgan, S. G. (2017). Numerical simulations of onshore transport of larvae and

detritus to a steep pocket beach. *Mar. Ecol. Prog. Ser.* 582, 33–43. doi: 10.3354/meps12331

Fujimura, A. G., Reniers, A. J. H. M., Paris, C. B., Shanks, A. L., MacMahan, J. H., and Morgan, S. G. (2018). Mechanisms of cross-shore transport and spatial variability of phytoplankton on a rip-channeled beach. *Front. Mar. Sci.* 5. doi: 10.3389/fmars.2018.00183

Fujita, Y., Kimura, T., Atsuo, S., Shiori, A., and Naruse, T. (2012). Typhoon damage of large-scaled coral communities dominated by *Acropora horrida* (Dana 1846) (Scleractinia: acroporidae) in the mesophotic zone off kumejima island, the Ryukyu islands, Japan. *Biol. Mag. Okinawa* 50, 61–66.

Garavelli, L., Studivan, M. S., Voss, J. D., Kuba, A., Figueiredo, J., and Cherubin, L. M. (2018). Assessment of mesophotic coral ecosystem connectivity for proposed expansion of a marine sanctuary in the northwest gulf of Mexico: larval dynamics. *Front. Mar. Sci.* 5. doi: 10.3389/fmars.2018.00174

Glynn, P. W. (1996). Coral reef bleaching: facts, hypotheses and implications. *Global Change Biol.* 2, 495–509. doi: 10.1111/j.1365-2486.1996.tb00063.x

Graham, N. A. J., Wilson, S. K., Pratchett, M. S., Polunin, N. V., and Spalding, M. D. (2009). Coral mortality versus structural collapse as drivers of corallivorous butterflyfish decline. *Biodivers. Conserv.* 18, 3325–3336. doi: 10.1007/s10531-009-9633-3

Hearn, C. J. (1999). Wave-breaking hydrodynamics within coral reef systems and the effect of changing relative sea level. *J. Geophys. Res. Oceans* 104, 30007–30019. doi: 10.1029/1999JC900262

Hench, J. L., Leichter, J. J., and Monismith, S. G. (2008). Episodic circulation and exchange in a wave-driven coral reef and lagoon system. *Limnol. Oceanogr.* 53 (6), 2681–2694. doi: 10.4319/lo.2008.53.6.2681

Hinderstein, L. M., Marr, J. C. A., Martinez, F. A., Dowgiallo, M. J., Puglise, K. A., Pyle, R. L., et al. (2010). Theme section on "Mesophotic coral ecosystems: characterization, ecology, and management". *Coral Reefs* 29, 247–251. doi: 10.1007/s00338-010-0614-5

Hoegh-Guldberg, O., Mumby, P. J., Hooten, A. J., Steneck, R. S., Greenfield, P., Gomez, E., et al. (2007). Coral reefs under rapid climate change and ocean acidification. *Science* 318, 1737–1742. doi: 10.1126/science.1152509

Hoegh-Guldberg, O., Poloczanska, E. S., Skirving, W., and Dove, S. (2017). Coral reef ecosystems under climate change and ocean acidification. *Front Mar. Sci.* 4. doi: 10.3389/fmars.2017.00158

Holstein, D. M., Paris, C. B., Vaz, A. C., and Smith, T. B. (2016). Modeling vertical coral connectivity and mesophotic refugia. *Coral Reefs* 35, 23–37. doi: 10.1007/s00338-015-1339-2

Hughes, T. P., Anderson, K. D., Connolly, S. R., Heron, S. F., Kerry, J. T., Lough, J. M., et al. (2018). Spatial and temporal patterns of mass bleaching of corals in the anthropocene. *Science* 359, 80–83. doi: 10.1126/science.aan8048

Hughes, T. P., Kerry, J. T., Álvarez-Noriega, M., Álvarez-Romero, J. G., Anderson, K. D., Baird, A. H., et al. (2017). Global warming and recurrent mass bleaching of corals. *Nature* 543, 373–377. doi: 10.1038/nature21707

Hughes, T. P., and Tanner, J. E. (2000). Recruitment failure, life histories, and long-term decline of Caribbean corals. *Ecology* 81, 2250–2263. doi: 10.1890/0012-9658(2000)081[2250:RFLHAL]2.0.CO;2

Ikeda, E., Iryu, Y., Sugihara, K., Ohba, H., and Yamada, T. (2006). Bathymetry, biota and sediments on the hirota reef, tane-ga-shima–the northernmost coral reef in the Ryukyu islands. *Isl. Arc* 15 (4), 407–419. doi: 10.1111/j.1440-1738.2006.00538.x

Iwasaki, S., Isobe, A., Kako, S., Uchida, K., and Tokai, T. (2017). Fate of microplastics and mesoplastics carried by surface currents and wind waves: a numerical model approach in the Sea of Japan. *Mar. pollut. Bull.* 121, 85–96. doi: 10.1016/j.marpolbul.2017.05.057

Kahng, S. E., Copus, J. M., and Wagner, D. (2014). Recent advances in the ecology of mesophotic coral ecosystems (MCEs). *Curr. Opin. Environ. Sustainability* 7, 72–81. doi: 10.1016/j.cosust.2013.11.019

Kahng, S. E., Garcia-Sais, J. R., Spalding, H. L., Brokovich, E., Wagner, D., Weil, E., et al. (2010). Community ecology of mesophotic coral reef ecosystems. *Coral Reefs* 29, 255–275. doi: 10.1007/s00338-010-0593-6

Kamidaira, Y., Kawamura, H., Kobayashi, T., and Uchiyama, Y. (2019). Development of regional downscaling capability in STEAMER ocean prediction system based on multi-nested ROMS model. *J. Nucl. Sci. Tech.* 56 (8), 752–763. doi: 10.1080/00223131.2019.1613269

Kamidaira, Y., Uchiyama, Y., Kawamura, H., Kobayashi, T., and Furuno, A. (2018). Submesoscale mixing on initial dilution of the radionuclides released from the fukushima dai-ichi nuclear power plant. *J. Geophys. Res. Oceans* 123, 4, 2808–2828. doi: 10.1002/2017JC013359

Kamidaira, Y., Uchiyama, Y., Kawamura, H., Kobayashi, T., and Otosaka, S. (2021). A modeling study on the oceanic dispersion and sedimentation of radionuclides off the coast of fukushima. *J. Environ. Radioact.* 106724, 238–239. doi: 10.1016/j.jenvrad.2021.106724

Kamidaira, Y., Uchiyama, Y., and Mitarai, S. (2017). Eddy-induced transport of the kuroshio warm water around the Ryukyu islands in the East China Sea. *Cont. Shelf Res.* 143, 206–218. doi: 10.1016/j.csr.2016.07.004

Kayanne, H., Suzuki, R., and Liu, G. (2017). Bleaching in the Ryukyu islands in 2016 and associated degree heating week threshold. galaxea. *J. Coral Reef Stud.* 19, 17–18. doi: 10.3755/galaxea.19.1_17

Kimura, T., Shimoike, K., Suzuki, G., Nakayoshi, I., Shioiri, A., Tabata, A., et al. (2011). Large Scale communities of *Acropora horrida* in the mesophotic zone off kume island, Okinawa. *J. Jpn. Coral Reef Soc* 13, 43–45. doi: 10.3755/jcrs.13.43

Kramer, N., Eyal, G., Tamir, R., and Loya, Y. (2019). Upper mesophotic depths in the coral reefs of eilat, red Sea, offer suitable refuge grounds for coral settlement. *Sci. Rep.* 9, 1–12. doi: 10.1038/s41598-019-38795-1

Kurosawa, K., Uchiyama, Y., and Kosako, T. (2020). Development of a numerical marine weather routing system for coastal and marginal seas using regional oceanic and atmospheric simulations. *Ocean Eng.* 195, 106706. doi: 10.1016/j.oceaneng.2019.106706

Lafratta, A., Fromont, J., Speare, P., and Schönberg, C. H. L. (2016). Coral bleaching in turbid waters of north-western Australia. *Mar. Freshw. Res.* 68 (1), 65–75. doi: 10.1071/MF15314

Lesser, M. P., Slattery, M., and Leichter, J. J. (2009). Ecology of mesophotic coral reefs. *J. Exp. Mar. Biol. Ecol.* 375 (1–2), 1–8. doi: 10.1016/j.jembe.2009.05.009

Lowe, R. J., Falter, J. L., Monismith, S. G., and Atkinson, M. J. (2009). Wave-driven circulation of a coastal reef–lagoon system. *J. Phys. Oceanogr.* 39, 873–893. doi: 10.1175/2008JPO3958.1

Marchesiello, P., Benshila, R., Almar, R., Uchiyama, Y., McWilliams, J., and Shchepetkin, A. (2015). On tridimensional rip current modeling. *Ocean Modell.* 96 (1), 36–48. doi: 10.1016/j.ocemod.2015.07.003

Mason, E., Molemaker, J., Shchepetkin, A. F., Colas, F., McWilliams, J. C., and Sangrà, P. (2010). Procedures for offline grid nesting in regional ocean models. *Ocean Model.* 35, 1–15. doi: 10.1016/j.ocemod.2010.05.007

Masunaga, E., Uchiyama, Y., Suzue, Y., and Yamazaki, H. (2018). Dynamics of internal tides over a shallow ridge investigated with a high-resolution downscaling regional ocean model. *Geophys. Res. Lett.* 45 (8), 3550–3558. doi: 10.1002/2017GL076916

Masunaga, E., Uchiyama, Y., Zhang, X., Kimura, W., and Kosako, T. (2022). Modulation of submesoscale eddies and associated Lagrangian transport due to tides and shallow ridge along the kuroshio. *Deep-Sea Res. Part I* 186, 103828. doi: 10.1016/j.dsr.2022.103828

Matsushita, K., Uchiyama, Y., Takaura, N., and Kosako, T. (2022). Fate of river-derived microplastics from the south China Sea: sources to surrounding seas, shores, and abysses. *Environ. pollut.* 308, 119631. doi: 10.1016/j.envpol.2022.119631

Menza, C., Kendall, M., and Hile, S. (2008). The deeper we go the less we know. *Rev. Biol. Trop.* 56, 11–14. doi: 10.15517/rbt.v56i0.5575

Mitarai, S., Siegel, D. A., Watson, J. R., Dong, C., and McWilliams, J. C. (2009). Quantifying connectivity in the coastal ocean with application to the southern California bight. *J. Geophys. Res. Oceans* 114, 21. doi: 10.1029/2008JC005166

Miyazawa, Y., Zhang, R., Guo, X., Tamura, H., Ambe, D., Lee, J.-S., et al. (2009). Water mass variability in the western north pacific detected in a 15- year eddy resolving ocean reanalysis. *J. Oceanogr.* 65, 737–756. doi: 10.1007/s10872-009-0063-3

Munday, P. L., Leis, J. M., Lough, J. M., Paris, C. B., Kingsford, M. J., Berumen, M. L., et al. (2009). Climate change and coral reef connectivity. *Coral Reefs* 28, 379–395. doi: 10.1007/s00338-008-0461-9

Munk, W. H., and Sargent, M. C. (1948). Adjustment of bikini atoll to ocean waves. *Eos Trans. Am. Geophysical Union* 29, 855–860. doi: 10.1029/TR029i006p00855

Nishikawa, A., Katoh, M., and Sakai, K. (2003). Larval settlement rates and gene flow of broadcast-spawning (*Acropora tenuis*) and planula-brooding (*Stylophora pistillata*) corals. *Mar. Ecol. Prog. Ser.* 256, 87–97. doi: 10.3354/meps256087

Ohara, T., Fujii, T., Kawamura, I., Mizuyama, M., Montenegro, J., Shikiba, H., et al. (2013). First record of a mesophotic *Pachyseris foliosa* reef from Japan. *Mar. Biodiv.* 43, 71–72. doi: 10.1007/s12526-012-0137-0

Rodríguez, E., Morris, C. S., Belz, J. E., Chapin, E. C., Martin, J. M., Daffer, W., et al. (2005). "An assessment of the SRTM topographic products," in *Technical report JPL* (Pasadena, California, U.S: Jet Propulsion Laboratory), 143. D-31639.

Romero, L., Siegel, D. A., McWilliams, J. C., Uchiyama, Y., and Jones, C. (2016). Characterizing stormwater dispersal and dilution from small coastal streams. *J. Geophys. Res. Oceans* 121, 3926–3943. doi: 10.1002/2015JC011323

Romero, L., Uchiyama, Y., Ohlmann, C., McWilliams, J. C., and Siegel, D. A. (2013). Particle-pair dispersion in the southern California coastal zone. *J. Phys. Oceanogr.* 43, 1862–1879. doi: 10.1175/JPO-D-13-011.1

Shchepetkin, A. F., and McWilliams, J. C. (2005). The regional ocean modeling system (ROMS): a split-explicit, free-surface, topography-following-coordinate oceanic model. *Ocean Modell.* 9, 347–404. doi: 10.1016/j.ocemod.2004.08.002

Shchepetkin, A. F., and McWilliams, J. C. (2008). "Computational kernel algorithms for fine-scale, multiprocess, longtime oceanic simulations," in *Handbook of numerical analysis: computational methods for the ocean and the atmosphere*. Eds. R. Temam and J. Tribbia (Amsterdam: Elsevier), 119–181. doi: 10.1016/S1570-8659(08)01202-0

Shlesinger, Y., and Loya, Y. (1985). Coral community reproductive patterns: red Sea versus the great barrier reef. *Science* 228, 1333–1335. doi: 10.1126/science.228.4705.1333

Sinniger, F., and Harii, S. (2018). "Studies on mesophotic coral ecosystems in Japan," in *Coral reef studies of Japan* (Singapore: Springer), 149–162. doi: 10.1007/978-981-10-6473-9_10

Sinniger, F., Morita, M., and Harii, S. (2013). "Locally extinct" coral species *Seriatopora hystrix* found at upper mesophotic depths in Okinawa. *Coral Reefs* 32, 153. doi: 10.1007/s00338-012-0973-1

Sinniger, F., Prasetia, R., Yorifuji, M., Bongaerts, P., and Harii, S. (2017). *Seriatopora* Diversity preserved in upper mesophotic coral ecosystems in southern Japan. *Front. Mar. Sci.* 4. doi: 10.3389/fmars.2017.00155

Slattery, M., Lesser, M. P., Brazeau, D., Stokes, M. D., and Leichter, J. J. (2011). Connectivity and stability of mesophotic coral reefs. *J. Exp. Mar. Biol. Ecol.* 408, 32–41. doi: 10.1016/j.jembe.2011.07.024

Symonds, G., Black, K. P., and Young, I. R. (1995). Wave-driven flow over shallow reefs. *J. Geophys. Res. Oceans* 100, 2639–2648. doi: 10.1029/94JC02736

Szmant, A. M., and Meadows, M. G. (2006). Developmental changes in coral larval buoyancy and vertical swimming behavior: implications for dispersal and connectivity. in. *Proc. 10th Int. Coral Reef Symp.*, 431–437.

Tada, H., Uchiyama, Y., and Masunaga, E. (2018). Impacts of two super typhoons on the kuroshio and marginal seas on the pacific coast of Japan. *Deep-Sea Res. Part I* 132, 80–93. doi: 10.1016/j.dsr.2017.12.007

Takeda, N., Kashima, M., Odani, S., Uchiyama, Y., Kamidaira, Y., and Mitarai, S. (2021). Identification of coral spawn source areas around sekisei lagoon for recovery and poleward habitat migration by using a particle-tracking model. *Sci. Rep.* 11, 6963. doi: 10.1038/s41598-021-86167-5

Thomas, C. J., Bridge, T. C. L., Figueiredo, J., Deleersnijder, E., and Hanert, E. (2015). Connectivity between submerged and near-sea-surface coral reefs: can submerged reef populations act as refuges? *Diversity Distrib.* 21, 1254–1266. doi: 10.1111/ddi.12360

Uchiyama, Y., Kanki, R., Takano, A., Yamazaki, H., and Miyazawa, Y. (2018a). Mesoscale reproducibility in regional ocean modeling with a 3-d stratification estimate based on aviso-argo data. *Atmosphere-Ocean* 56 (4), 212–229. doi: 10.1080/07055900.2017.1399858

Uchiyama, Y., McWilliams, J. C., and Akan, C. (2017a). Three-dimensional transient rip currents: bathymetric excitation of low-frequency intrinsic variability. *J. Geophys. Res. Oceans* 122, 5826–5849. doi: 10.1002/2017JC013005

Uchiyama, Y., McWilliams, J. C., and Restrepo, J. M. (2009). Wave-current interaction in nearshore shear instability analyzed with a vortex force formalism. *J. Geophys. Res. Oceans* 114, C6. doi: 10.1029/2008JC005135

Uchiyama, Y., McWilliams, J. C., and Shchepetkin, A. F. (2010). Wave-current interaction in an oceanic circulation model with a vortex force formalism: application to the surf zone. *Ocean Model.* 34 (1–2), 16–35. doi: 10.1016/j.ocemod.2010.04.002

Uchiyama, Y., Miyagawa, T., Odani, S., and Mitarai, S. (2018b). A Lagrangian analysis on coastal dispersal of coral larvae and spawn around Okinawa island, Japan. *J. Japan Soc Civil Eng. Ser. B2 (Coastal Engineering)* 74 (2), I_1291–I_1296. doi: 10.2208/kaigan.74.I_1291

Uchiyama, Y., Odani, S., Kashima, M., Kamidaira, Y., and Mitarai, S. (2018c). Influences of the kuroshio on interisland remote connectivity of corals across the nansei archipelago in the East China Sea. *J. Geophys. Res. Oceans* 123 (12), 9245–9265. doi: 10.1029/2018JC014017

Uchiyama, Y., Suzue, Y., and Yamazaki, H. (2017b). Eddy-driven nutrient transport and associated upper-ocean primary production along the kuroshio. *J. Geophys. Res. Oceans* 122, 5046–5062. doi: 10.1002/2017JC012847

Uchiyama, Y., Tokunaga, N., Aduma, K., Kamidaira, Y., Tsumune, D., Iwasaki, T., et al. (2022). A storm-induced flood and associated nearshore dispersal of the river-derived suspended ^{137}Cs. *Sci. Total Environ.* 816, 151573. doi: 10.1016/j.scitotenv.2021.151573

Uchiyama, Y., Zhang, X., Suzue, Y., Kosako, T., Miyazawa, Y., and Nakayama, A. (2018d). Residual effects of treated effluent diversion on a seaweed farm in a tidal strait using a multi-nested high-resolution 3-d circulation-dispersal model. *Mar. pollut. Bull.* 130, 40–54. doi: 10.1016/j.marpolbul.2018.03.007

Van Oppen, M. J., Bongaerts, P. I. M., Underwood, J. N., Peplow, L. M., and Cooper, T. F. (2011). The role of deep reefs in shallow reef recovery: an assessment of vertical connectivity in a brooding coral from west and east Australia. *Mol. Ecol.* 20 (8), 1647–1660. doi: 10.1111/j.1365-294X.2011.05050.x

van Woesik, R., Sakai, K., Ganase, A., and Loya, Y. J. M. E. P. S. (2011). Revisiting the winners and the losers a decade after coral bleaching. *Mar. Ecol. Prog. Ser.* 434, 67–76. doi: 10.3354/meps09203

Vermeij, M. J. A., Fogarty, N. D., and Miller, M. W. (2006). Pelagic conditions affect larval behavior, survival, and settlement patterns in the Caribbean coral *Montastraea faveolata*. *Mar. Ecol. Prog. Ser.* 310, 119–128. doi: 10.3354/meps310119

Wang, P., McWilliams, J. C., and Uchiyama, Y. (2021). A nearshore oceanic front induced by wave streaming. *J. Phys. Oceanogr.* 51 (2), 1967–1984. doi: 10.1175/JPO-D-21-0004.1

Wang, P., McWilliams, J. C., Uchiyama, Y., Chekroun, M. D., and Yi, D. L. (2020). Effects of wave streaming and wave variations on nearshore wave-driven circulation. *J. Phys. Oceanogr.* 50 (10), 3025–3041. doi: 10.1175/JPO-D-19-0304.1

Weir, B., Uchiyama, Y., Lane, E. M., Restrepo, J. M., and McWilliams, J. C. (2011). A vortex force analysis of the interaction of rip currents and surface gravity waves. *J. Geophys. Res. Oceans* 116, C5. doi: 10.1029/2010JC006232

Zhang, X., Uchiyama, Y., Masunaga, E., Suzue, Y., and Yamazaki, H. (2022). Seasonal variability of upper ocean primary production along the kuroshio off Japan: roles of eddy-driven nutrient transport. *Front. Mar. Sci.* 9. doi: 10.3389/fmars.2022.990559

Zhang, X., Uchiyama, Y., and Nakayama, A. (2019). On relaxation of the influences of treated sewage effluent on an adjacent seaweed farm in a tidal strait. *Mar. pollut. Bull.* 144, 265–274. doi: 10.1016/j.marpolbul.2019.04.050